Supercond. Sci. Technol. 10 (1997) 169–185. Printed in the UK PII: S0953-2048(97)77270-1

TOPICAL REVIEW

High-temperature superconducting thick films

N McN Alford†, S J Penn† and T W Button‡

† South Bank University, 103 Borough Road, London SE1 0AA, UK
‡ IRC in Materials, University of Birmingham, Birmingham B15 2TT, UK

Received 20 August 1996, in final form 27 January 1997

Abstract. High-temperature superconducting (HTS) thick films have undergone a period of rapid progress since their discovery in 1986. In this review thick-film materials are described with special reference to their processing, their properties and the development of devices. The devices include HTS magnetic shields, resonators for microwave filters, antennas and wire. The translation of science into applications has taken place in a relatively short time and already impressive performance is seen in HTS prototype devices.

1. Introduction

The use of thick films in the European electronics industry constitutes a business of some 1.42 billion ECU (1994). The hybrid market is around 2.9 billion ECU (1994) and for comparison the market for thin films in Europe was 265 million ECU in 1994 (N Sinandury, TWI, personal communication). The development of superconducting thick films is an essential component in the growth of the superconducting electronics industry. This paper will review the materials, the deposition and manufacturing techniques and the devices associated with high-temperature superconducting (HTS) thick films.

1.1. Definitions

It is important at the outset of this paper to define precisely what is meant by the term thick film in order to avoid confusion. The term relates not so much to the thickness of films but to the mode of deposition. In the electronics industry a thick-film conductor of silver, copper or gold, for example, is prepared by taking a powder of the metal and mixing the powder with a vehicle. The vehicle is a mixture of polymers and solvents which are thoroughly mixed with the chosen powder, usually on a three-roll mill, until a homogeneous mixture is formed. This mixture is known as an ink. The ink is then deposited onto a suitable substrate, for example polycrystalline alumina or polymer circuit board, by screen printing and then, in the case of ceramic substrates, fired at high temperature in order to sinter the particles in the ink so that a homogeneous electrical circuit is obtained. This differs from thin-film methods such as sputtering, laser ablation, chemical vapour deposition, evaporation etc in three very important respects. First, thin-film deposition usually requires the use of single-crystal substrates, second thin films are usually deposited with the intention of achieving a degree of epitaxy with respect to the crystallographic orientation of the substrate and third thin films usually require the use of vacuum technology. The most important distinction, however, is the deposition method.

In the literature the term thick films is unfortunately used somewhat loosely to refer to thin-film deposition methods which have built up many layers of a compound so that effectively a 'thick' thin film results. In this review this is classed as a thin film. A good example of this is the use of thin-film deposition techniques to produce films which can be up to several micrometres thick for current-carrying conductors. For example Wu *et al* [1] have produced thin films on flexible nickel substrates with YSZ buffer layers by ion-beam-assisted deposition (pulsed-laser deposition) and have achieved very high critical currents using this process. This is discussed at the end of this review.

In summary, thick films are produced by preparing an ink from a powder while thin films are usually produced by methods which encourage epitaxy onto a single-crystal substrate. Within these broad definitions there are variants such as sol–gel, electrodeposition and solution-spraying techniques.

Table 1. Transition temperatures of the major HTS systems used in thick-film applications.

Material	T_c (K)
YBCO	93
BSCCO 2212	85
BSCCO 2223	110
TBCCO 2212	98
TBCCO 2223	125
HgBaCaCu 1223	164 (under pressure)

0953-2048/97/040169+17$19.50

Bulk materials are classified as HTS materials made by powder routes and which may be free-standing objects such as discs, tubes or rods or may be produced by encapsulating the powder in a substrate such as silver and drawn into a tape or wire [2–4]. The commonest method for producing conductors is by the powder-in-tube (PIT) method [2–4] in which a superconductor powder is placed inside a silver tube and swaged and/or rolled into the desired conductor shape. However, another technique which is also used is the deposition of a superconductor thick film paste or slurry onto a metallic (silver) substrate. In a variant, the superconductor may be deposited onto a barrier layer such as zirconia which itself is on a metallic substrate, e.g. a high temperature nickel alloy. This is classed as a thick film and conductors made by these methods are referred to as having been prepared by 'open' methods as opposed to 'closed' methods such as PIT. Such conductors have been shown to possess excellent properties which will be discussed below.

2. Thick films

2.1. Materials and methods for thick-film superconductors

The most commonly reported materials are thick films of $YBa_2Cu_3O_x$ (YBCO, 123) [5–10], TlBaCaCuO (TBCCO 2223, 2212) [11–15] and Bi(Pb)SrCaCuO (BSCCO 2223, 2212) [16–20]. Although relatively little work has been carried out on thick films of the mercury system ($HgBa_2Ca_2Cu_3O_{8+\delta}$) these are also included. The T_c of these materials are given in table 1.

Adjustments to the stoichiometry of these three main systems have also been reported. In general conductors are made with films of BSCCO or TBCCO taking advantage of the anisotropy in crystal morphology and current-carrying capacity, which is greatest in the a–b plane. R.f. and microwave devices are more commonly made from YBCO thick films as these have been shown to possess a consistently lower surface resistance (R_s) [5, 6] than films made with BSCCO or TBCCO. There is a wide variety of methods employed to obtain the thick films; for example spray pyrolysis has been used coat substrates and electrophoretic deposition has also been used to coat r.f. cavities using silver substrates but the commonest techniques are screen printing or doctor blading, widely used in the electronics industry. The modes of manufacture follow broadly similar principles.

As an example we shall examine the preparation of YBCO thick films. In common with almost all thick-film preparations, the starting point is the superconductor powder which is conveniently made by a mixed-oxide route. The raw materials usually used, yttrium oxide, barium carbonate and copper oxide, are weighed out into the appropriate stoichiometric proportions [5–7]. These are mixed in a ball mill or a vibroenergy mill in alcohol for 16 h and dried in a rotary evaporator. The mixed powder is then calcined in an air furnace. The process of calcination takes place below the melting temperature of the constituents and because only few point contacts exist in a powder bed the process is often repeated until a homogeneous compound is attained. The resultant material is a friable 'crumble' which must be ground to a fine powder in alcohol in a ball mill or vibroenergy mill using ceramic (e.g. zirconia) milling media. This is again dried in a rotary evaporator. The resulting powder is then made into an ink by three-roll milling using polymers and solvents. The ink is a viscous material which can be screen printed or 'doctor bladed' onto a suitable substrate. If spin coating is employed as a deposition technique then the viscosity must be adjusted accordingly. The temperatures of calcination are typically 900 °C for YBCO, and closer to 800 °C for BSCCO and TBCCO. TBCCO is unusual in that the thallium is often incorporated in a second-stage process, e.g. as thallium oxide vapour, in order to minimize toxicity problems and difficulties associated with loss of thallium due to vaporization.

2.2. Materials for substrates

The substrate performs an important function in supporting the film. The key properties of a substrate for thick films are first that it should not react deleteriously with the superconductor film and second that it should maintain shape at the processing temperature of the superconductor. In patterned films where the substrate is exposed to a r.f. or microwave field there are other important considerations, the most important of which is that the dielectric loss should be low which generally means that the dielectric constant is moderate at 30 or below. Finally the issue of cost is important. Table 2 shows some ceramic materials which have been used for thick-film substrates. Some of the commonly used thin-film substrate materials such as $LaAlO_3$ and buffered Al_2O_3 are generally unsuitable as substrates for thick films owing to the higher processing temperatures required for the thick-film process (in the ranges 900–1100 °C for YBCO, 830–900 °C for BSCCO and TBCCO), which causes rapid diffusion of species from the substrate to the superconductor with an adverse effect on superconducting properties. The presence of a liquid phase during sintering and a certain degree of reaction with the substrate is beneficial as it causes good adhesion with the substrate. However, there is a balance between the degree of reaction needed to provide adhesion and that which causes a deleterious reduction in the superconducting properties. Other substrate materials such as $Sr(Al_{0.5}Ta_{0.5})O_3$ and $Sr(Al_{0.5}Nb_{0.5})$ are under consideration as thin-film substrates and $LaSrGaO_4$ has also been tested as a possible candidate for thin films. They have not so far been assessed for thick-film applications. Recently, Koshy and coworkers [21–30] have made significant advances in the development of materials for substrates, some of which are presented in table 2. Measurements of $\tan\delta$ and dielectric constant were made in our laboratory in an oxygen-free copper cylindrical cavity with a vertically adjustable top plate. The dielectric pucks were placed on a low-loss, low-permittivity quartz spacer. The transmission measurements were performed using an HP8719 vector network analyser with 1 Hz resolution.

Table 2. Properties of candidate materials for HTS thick-film substrates (single-crystal values added for information).

Substrate material	Dielectric constant ε'	Dielectric loss ($\tan\delta$) at 300 K	Frequency f	Adverse reaction with thick film HTS > 1000 °C
Y-stabilized zirconia (this work)	25	10^{-3}	7.5 GHz	No
MgO	10	ND[a]		Yes
Al_2O_3 (this work)	9.5	2.2×10^{-5}	10 GHz	Yes
$GdBa_2HfO_{5.5}$ [27]	20	5×10^{-3}	10 MHz	No
$(Pr, Sm, Gd)Ba_2SbO_6$ [24]	12–16	$(8–25)\times10^{-4}$	10 MHz	No
$YBa_2SnO_{5.5}$ [21]	10	0.05	10 MHz	No
YBa_2NbO_6 (this work)	33	1.4×10^{-4}	4.9 GHz	No [28]
$PrBa_2NbO_6$ [23]	15	2×10^{-4}	10 MHz	No
$NdBa_2NbO_6$ (this work)	42	7.4×10^{-4}	4.4 GHz	No [23]
$SmBa_2NbO_6$ [23]	9	1×10^{-4}	10 MHz	No
$EuBa_2NbO_6$ [23]	11	2×10^{-4}	10 MHz	No
$BaZrO_3$ (this work) (at 90% of full density)	12	2.5×10^{-4}	8 GHz	No [29]
$BaHfO_3$ [29]	ND[a]	ND[a]		No
$LaAlO_3$ (this work) (at 96% of full density)	21	4×10^{-4}	8 GHz	Yes
Single crystals				
Al_2O_3 (this work)	9.5	10^{-5}	8.5 GHz	
MgO (this work)	9	10^{-5}	7.35 GHz	
$LaAlO_3$ (this work)	22.6	2.3×10^{-5}	7.34 GHz	
TiO_2 (this work)	100	1.4×10^{-4}	8.6 GHz	

[a] ND = not determined.

At present, the preferred substrate for microwave applications for availability, cost and properties is yttria-stabilized zirconia. Materials for thick-film HTS are preferably polycrystalline ceramics which can be made as large-area planar or curved substrates at low cost. In general the dielectric constant is not greatly affected by reducing the temperature of measurement but the dielectric loss is often reduced considerably at low temperatures. This is the subject of further investigation in our laboratories.

2.3. Metals used as thick-film substrates

For conductors in particular there has been a good deal of interest in using metals as a substrate for thick films. The superconducting materials used for such conductors are either BSCCO or TBCCO which may be processed at a lower temperature than YBCO and hence the constraints on the choice of metal are not as severe. Silver (and some silver alloys) does not display a deleterious reaction with any of the three systems and has been used extensively.

Battacharya *et al* [31] have used electrophoretic deposition to deposit films of YBCO on silver and have observed extensive grain growth and recrystallization. They also observed a thickness dependence for the critical current density (J_c) with a J_c of 450 A cm^{-2} (77 K, $H = 0$) for films 65 μm thick and $J_c > 4000$ A cm^{-2} for films 3 μm thick. Masuda *et al* [32] found that by using sols prepared from alkoxides J_c of up to 1.18×10^4 A cm^{-2} were obtained at 77 K in zero magnetic field. They found also that the melt processing in the peritectic reaction regime was beneficial. Ezura *et al* [33] used low-pressure plasma spraying to deposit YBCO thick films onto silver- or nickel-buffered copper substrates and measured the surface resistance (R_s) at 3 GHz. R_s was found to be less than that of copper at 77 K but inferior to results obtained on zirconia substrates [5] as a consequence of HTS–substrate reaction. Nickel alloys such as Inconel 600 and Inconel X have been examined by Schulz *et al* [34]. They spray-pyrolysed YBCO onto the substrates and found that pre-reacted YBCO was preferable to aqueous metal nitrate solutions. They experienced severe difficulties because of substrate interactions. Vanolo *et al* [35] deposited YBCO using nickel-based buffer layers on stainless steel containing chromium and found that the shielding effectiveness was comparable with that of shields made by depositing YBCO on silver. The main problem was oxygenation of the YBCO [35]. Os'kina *et al* [36] have deposited BSCCO thick films on nickel substrates with silver or gold interlayers. They did not observe any appreciable reaction between the interlayer and the BSCCO. BSCCO 2223 attained a transition temperature T_c ($R = 0$) of 92 K, 101 K and 99 K on gold, silver and nickel with a silver buffer layer respectively. The use of thin-film deposition methods to produce conductors on nickel alloy substrates is discussed in more detail in section 3.

2.4. Sintering of HTS thick films

Each of the main systems sinters in a different manner but again the principles are the same. Once a film has been deposited onto the substrate the particles of superconductor powder must be encouraged to coalesce to form a uniform thick film. The driving force for sintering is the reduction of surface energy by the reduction of surface area and this is achieved by reaction of the particles at high temperature. The reduction of surface area is achieved by material transport. If we imagine two spherical particles of radii r, then the contact between the particles will be characterized

by a contact diameter x. In the initial stages of sintering the surface curvature at the contact between the two particles is directly related to the vapour pressure which is far higher in areas of high surface curvature. Initial-stage sintering is by evaporation and condensation.

However, in the sintering of HTS materials two main processes can be distinguished. The first is solid-state diffusion which occurs by vacancy migration and this is described by [37]

$$\frac{x}{r} = \left(\frac{40\gamma a^3 D^* t}{kT}\right)^{1/5} r^{3/5} \tag{1}$$

where γ is the surface energy, a^3 is the volume of the lattice vacancy, D^* is the diffusion coefficient and t is time. In thick films of all systems, however, it has been observed that sintering in the presence of a liquid phase is beneficial, and thus liquid-phase sintering is the second important process. In YBCO in particular the surface resistance and the current density are greatly improved if sintering takes place above the peritectic temperature (around 1030 °C in oxygen and 1020 °C in air) where there is both liquid and solid present as shown on the phase diagram (figure 1). Under these conditions the following equation [38,39] relating to viscous flow applies:

$$\frac{x}{r} = \left(\frac{3\gamma t}{2\nu r}\right)^{1/2} \tag{2}$$

where ν is the viscosity of the liquid phase. In YBCO thick films spherulitic grain growth is observed and grains with characteristic lengths of the order of millimetres are observed in samples sintered in the presence of a liquid phase. The kinetics of grain growth has been described by an isothermal grain growth model where the grain size l_g is related to a power law in time [40]:

$$l_g = At^n \tag{3}$$

where l_g is the grain size and A is a constant with an Arrhenius-type temperature dependence. The activation energy for YBCO is 125 kJ mol^{-1}. The exponent n has a value of 1/5 for a sintering temperature of say 930 °C with no liquid phase and of 1/3 when sintered above the peritectic temperature in the presence of a liquid phase (equations (1) and (2)). With reference to the phase diagram in figure 1 [41] (and [41–43]) it can be seen that, for YBCO in air, a peritectic reaction occurs at around 1000 °C. In such a reaction two phases, one of them a liquid, react to produce a new phase on cooling. 123 is not formed in equilibrium from the melt without the prior formation of 211. This is useful in two major respects. First the liquid encourages grain growth as was explained above and second the presence of small quantities of 211 encourages the formation of dislocations (caused by differential strain with respect to a 123 matrix) which aid pinning of the magnetic flux [44]. The liquid phase has a dramatic effect on the grain growth as shown in figures 2(*a*) (sintered below the peritectic temperature) and 2(*b*) (sintered above the peritectic temperature) and it also affects the performance (J_c, R_s) of the films. In HTS materials of all three systems

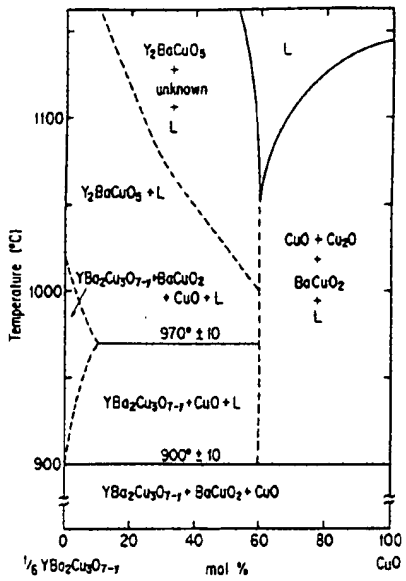

Figure 1. Temperature versus composition phase diagram for YBCO [41].

discussed in this review, the presence of a liquid phase is generally beneficial but great care must be taken in the time–temperature profile of the sintering step. In BSCCO 2223 for example, although a very small amount of liquid is beneficial, if the sintering temperature is too high the 2223 phase will be lost and BSCCO 2212 is the resultant phase. In fact, BSCCO 2212 is the preferred phase for some manufacturers of HTS wire because there is a wider processing window and because the properties ($J_c(H)$) of BSCCO 2212 at liquid-helium temperatures (and up to about 30 K) are preferred for current-carrying applications.

2.5. Current flow in thick films

The current flow characteristics in the three major materials systems are quite different in detail and this detail is principally related to the degree of anisotropy and the microstructure. The one characteristic which is common to all the systems is the influence of weak links on the critical current (J_c) and the magnetization characteristics.

2.5.1. YBCO. YBCO is the least anisotropic of the three systems. The current flow in YBCO melt-processed thick films has been studied in detail [45–47]. The observed length scale of current flow in melt-processed thick films is significantly greater than in those produced by sintering in the absence of a liquid phase, i.e. by solid-state sintering. The microstructure of the melt-processed YBCO films displays a characteristic spherulitic morphology which we have described as 'hub and spoke' [47]. The grains are characteristically 2 mm in diameter growing radially from a central, four-faceted hub. The strength of the link between the hub and spoke determines the intragrain J_c of the film and therefore plays an important role in determining the magnetic properties and the current transport of the films

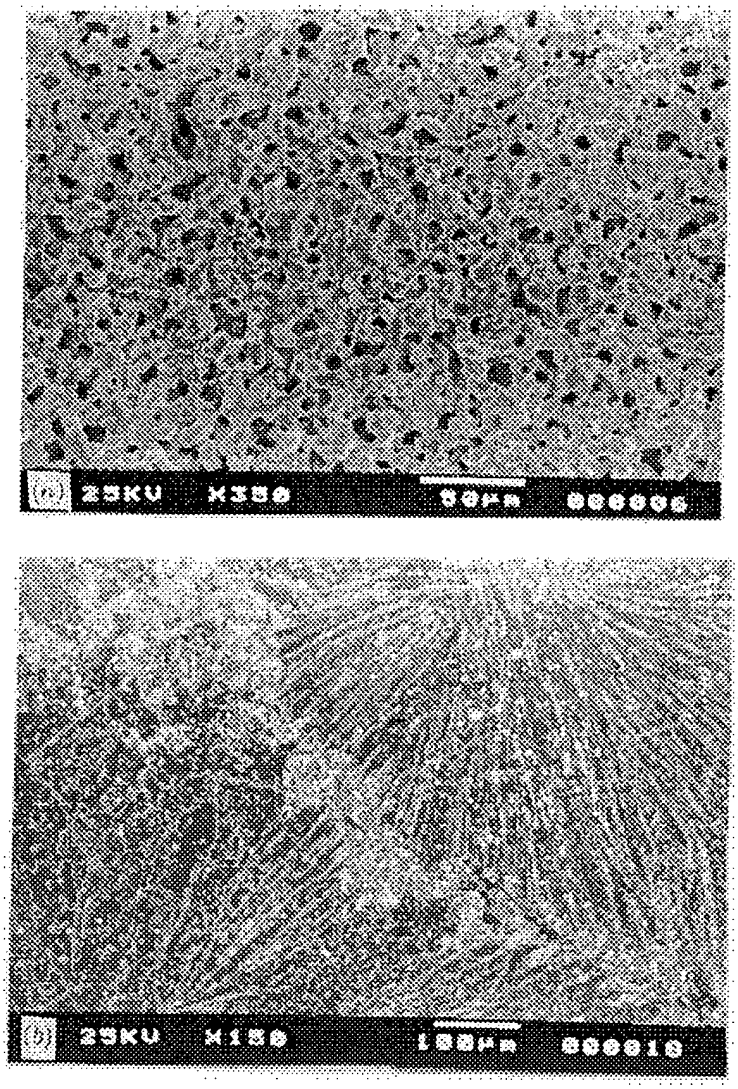

Figure 2. (*a*) Microstructure of YBCO sintered below the peritectic temperature. (*b*) Microstructure of YBCO sintered above the peritectic temperature.

and has led to the suggestion that the current is channelled through the central hub region as seen in figure 2(*b*). This suggestion [45] was shown to be correct when a series of experiments measurements were made before and after removal of the hub by mechanical abrasion. J_c (transport) before hub removal was 10^5 A cm^{-2} (0 T, 4.2 K) and 10^3 A cm^{-2} after hub removal (figure 3(*a*)) [45]. It has been found that thickness of the film plays an important role in controlling the microstructure, and hence the superconducting properties, with an optimum thickness in melt-processed YBCO films on zirconia of approximately 50 μm. Intergrain transport currents exist at very low levels in these films at 8 T (4.2 K) but intragrain transport J_c is around 10^4 A cm^{-2}.

The magnetic moment of the films is seen to scale with the cube of the sample width at 4.2 K, indicating that current flows on the length scale of the film (50 mm × 50 mm). Intragrain and intergrain magnetization measurements were calculated using the following equation and are shown in figure 3(*b*) [46]:

$$D_m = J_c t w^3 \qquad (4)$$

where w is the sample width, t is thickness, J_c is the critical current and D_m is the hysteresis width.

However, at temperatures above 70 K a critical state is not observed and above these temperatures the grains are only weakly coupled. Very low residual resistivity is observed in the films and this has been interpreted as indicative of clean grain boundaries. The main observations from the work on YBCO melt-processed thick films insofar as current-carrying properties are concerned are as follows.

(1) Below approximately 70 K the current flows over the dimensions of the sample, i.e. 50 mm × 50 mm, which are far greater than the grain dimensions (2 mm).

(2) Scaling is with the cube of sample width and agrees with the critical state model.

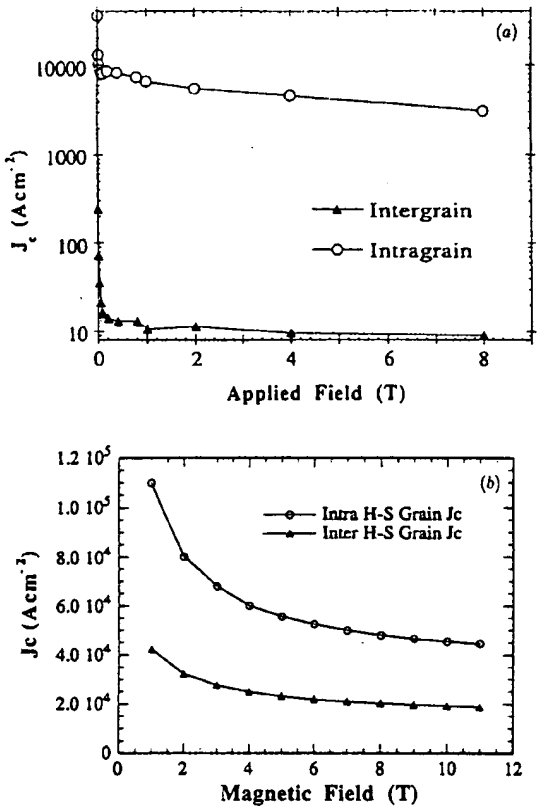

Figure 3. (*a*) Transport J_c versus B at 4.2 K for intergrain and intragrain measurements [45]. (*b*) Intragrain and intergrain hub–spoke critical current densities of YBCO melt-processed thick films as a function of applied field for 4.2 K magnetization measurements using equation (4) [46].

(3) A well-defined discontinuity in the magnetic moment versus sample width indicates the presence of well-defined intragrain and intergrain critical currents.

(4) At 77 K no scaling of the magnetization data was observed, indicating the absence of a critical state suggesting that the intergrain J_c is greatly diminished.

(5) The hub–spoke morphology is characteristic of good films. The current passes through the central hub.

The principal conclusion is that because the films' properties are strongly dependent on microstructure, any improvement in current-carrying performance will depend on further alteration of the microstructure. This will require a drastic change in the hub–spoke configuration. This is expected to be achieved through a modification of the temperature–time envelope to which the film is subjected during melt processing and will require the use of alternative substrate materials which do not react deleteriously. These modifications are in progress. Pt doping has been used successfully in bulk materials to increase the critical current and has also been shown to improve the properties of YBCO thick films [47]. Langhorn *et al* [48] showed that doping YBCO thick films with 0.1 wt% platinum powder caused an increase in the current-carrying capacity of the material from J_c = 1800 A cm^{-2} to J_c = 5000 A cm^{-2}. When 0.4 wt% $Ba_4Cu_{1-x}Pt_{2-x}O_{9-\delta}$ (0412) powder was added to the thick-film ink the properties improved, reaching $J_c > 7 \times 10^3$ A cm^{-2}. The presence of the 0412 powder, as with the Pt powder addition, caused a refinement (grain growth inhibition) of the 211 precipitates. This is believed to be beneficial as a result of the increased surface curvature of the 211 and its increased specific surface area leading to an enhanced dislocation density. TEM micrographs indicated increased dislocation densities at the 123–211 interface and it is believed that the dislocations themselves can act as flux-pinning sites.

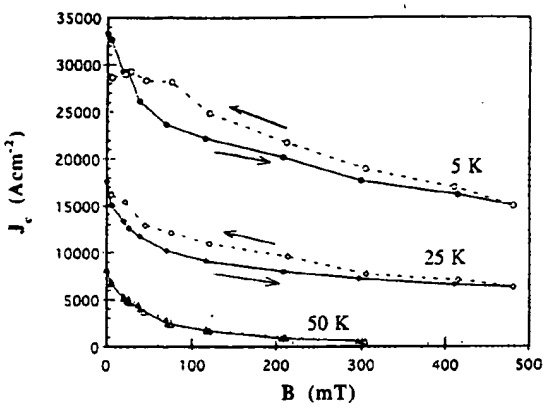

Figure 4. Transport J_c versus field for BSCCO thick films [49].

2.5.2. BSCCO. In BSCCO thick films similar effects are seen to those with the YBCO films described above. The J_c versus B curves at a constant temperature as shown in figure 4 [49] and J_c versus T curves at a constant field show a characteristic decrease in J_c with increasing field or temperature. The key factors responsible for the J_c behaviour are [49]

(1) breakdown of intergranular weak links with increasing field,

(2) reduced coupling between CuO layers producing a transition from vortex lines to vortex pancakes (three-dimensional (3D) to two-dimensional (2D) transition) and

(3) a variation in the effective pinning energy U_0, with field and temperature.

The shapes of the curves for transport J_c versus T and Δm versus T for constant B are very similar, indicating that the same mechanism may be controlling J_c in the two different measurements [49]. Single-crystal 2212 data show qualitatively the same behaviour. In general there appears to be a transition from 2D to 3D at around 50–100 mT. There is disagreement (Jones *et al* [49] and Yang *et al* [50]) in that some authors, e.g. Yang, indicate a transition at around 25 K, i.e. temperature dependent.

Holesinger *et al* [51] have used silver substrates to process BSCCO 2212 using an isothermal processing technique. In this process films are heated in an argon atmosphere at 10 °C min^{-1} to between 760 °C and 860 °C

and held for 1 h. The atmosphere is then changed to 10% O_2—90% Ar for 15 h. The sample is then cooled at 5 °C min^{-1} to room temperature. At 4 K the transport properties indicate that the samples processed at the higher temperatures, i.e. 860 °C, are less susceptible to an applied field of 1 T (parallel to *a–b* planes), dropping by only 20% of their self-field value, i.e. from $J_c = 2.87 \times 10^4$ A cm^{-2} to 2.26×10^4 A cm^{-2}. The highest J_c value was seen in samples processed at 780 °C, 1.2×10^5 A cm^{-2} but this dropped by around 40% to 7.38×10^4 A cm^{-2} in 1 T. The microstructure of these films consisted mainly of a series of grain colonies separated by low-angle grain boundaries. At 780 °C there was very little evidence of 2201 needles.

In a similar study Dimesso *et al* [52] examined the effects of annealing BSCCO 2212 on silver in an atmosphere of flowing nitrogen at temperatures between 300 °C and 700 °C for up to 6 h. The nitrogen atmosphere significantly reduces the melting temperature of the BSCCO 2212. At an anneal temperature of 500 °C T_c was found to be 85 K and J_c at 77 K was found to be 1600 A cm^{-2}. Unfortunately no transport data were available at 4 K.

BSCCO 2223 thick films pose problems in that the achievement of the three-layer 110 K 2223 phase is not straightforward and in particular there can be de-densification on annealing. Extra Ca and Cu has been found to be beneficial [53]. Pb substitution for Bi was observed by Takano *et al* [54] to lower the melting temperature and to favour the diffusion of species for the growth of the high-T_c phase. Finally, it is now well known that the addition of Ag [55, 56] influences the oxidation and annealing conditions, aids sintering, enhances J_c and encourages the formation of the high-T_c phase. The conditions which favour the formation of the high-T_c phase have been analysed by several authors. The starting composition is ideally copper rich, i.e. a 2224 composition; then it appears that a short time at a temperature between 870 and 900 °C, i.e. less than 1 h, followed by an extensive heat treatment of up to 100 h at around 860 °C is required for the formation of the 2223 phase [57].

2.5.3. TBCCO. TBCCO thick films which show significant promise have been prepared by spray pyrolysis of solution, ink spraying, electrodeposition and sol–gel. In this review we include such techniques for producing thick films since they satisfy the criteria that high-vacuum systems are not required, the precursors are powders of the appropriate oxides and the substrates do not need to be single crystals, although excellent results are reported on small samples grown on single crystals.

Schultz *et al* [58] have prepared TBCCO 1223 films by spray pyrolysis. These were prepared by taking a precursor powder ($Pb_{0.46}Ba_{0.4}Sr_{1.52}Ca_{1.86}Cu_3O_x$) of 4–6 μm in size, mixed with a vehicle binder and diluted with alcohol. This mixture was sprayed onto a heated (80–100 °C) substrate with an airbrush. The sample was then oxygen annealed at 700–800 °C for 60–75 min to remove the organics. The sample was sintered in a two-zone furnace at 770 °C for the separate thallium oxide source and 931 °C for the precursor for 2 h. The authors rank a series of substrates in order using morphology as a criterion, resulting in $LaAlO_3$ > $NdGaO_3$ > $SrTiO_3$ > MgO > YSZ which is approximately the ranking in lattice mismatch. Using magnetization measurements J_c was calculated to be 9×10^6 A cm^{-2} at 0 T, 5 K, and 2×10^6 A cm^{-2} at 4.75 T, 5 K.

The films were found to have a high degree of *c*-axis texture [59] but no macroscopic in-plane texture was found. The TEM of the grain boundaries revealed no second phase. There appears to be clustering of grain colonies which are locally aligned and where no large-angle grain boundaries exist. The authors suggest that there is long-range current transfer through a percolative network of small-angle colonies. This biaxial texture reduces the effect of weak links and may provide an effective means of using thick-film technology to prepare practical lengths of conductor in TBCCO.

The properties of thallium cuprate films for conductor applications are discussed in more detail in section 3.4.

2.5.4. Hg-1223. Tsabba and Reich [60] have prepared thick films of the Hg-1223 compound. They used aqueous (and glycerine) solutions into which were dissolved the nitrates of the Cu, Ca and Ba. After some hours a sol was formed to which was added Hg nitrate in an aqueous glycerine solution. The gel was spread onto a YSZ substrate and calcined at 900 °C for 10 min. These films were then sealed in helium-purged quartz ampoules in which were also sealed source pellets (HgO, BaO, CaO, CuO) of composition 1223. The ampoule was baked at around 870 °C for 2–3 h, annealed at 300 °C for 3 h and cooled in oxygen. The films obtained were 5–10 μm thick with no epitaxy and T_c was 110 K–117 K before oxygenation and 135 K after oxygenation. The resistive transition is broad but is centred around 135 K. Using magnetization measurements the authors calculate $J_c = 10^5$ A cm^{-2} at 10 K and 500 A cm^{-2} at 40 K at a grain size of 5 μm.

2.6. Surface impedance of HTS thick films

The variation in surface impedance results is enormous, reflecting the variation in the preparative methods and the quality of the thick films. Characterization methods used include cavity end wall replacement, all-HTS cavities, microstrip resonator techniques and dielectric resonator techniques. Of these the cavity end wall replacement and the dielectric resonator techniques are the most popular. Interest in the use of thick films for low surface impedance applications was given impetus when very low R_s was reported by [5, 6, 61] in YBCO. It was shown that R_s of melt-processed YBCO on zirconia substrates was significantly lower than for sintered materials and only a factor of 4 worse than for high-quality thin films. An advantage of the process is that very large areas and curved surfaces can be coated. The surface resistance at 7.5 GHz is 1.5 mΩ at 77 K and 0.75 mΩ at 64 K. The transport critical current density of such films is approximately 1000–2000 A cm^{-2} (77 K, 0 T) and 10^5 A cm^{-2} (4.2 K, 0 T). The materials of choice for low-R_s films are either YBCO, which has been extensively researched, or TBCCO which has recently been found to give low R_s values on zirconia substrates. R_s of BSCCO thick films has been found to be worse in comparison.

2.6.1. Advantages of thick films for low surface resistance applications. Unlike thin films where epitaxial growth is achieved, the deposition of HTS as a thick film onto polycrystalline substrates does not usually involve epitaxial growth. Nevertheless, the advantages of the thick film are as follows.

(1) Very large areas can be covered, e.g. 230 cm^2, with low R_s [5].

(2) Curved surfaces can be used and thus TE_{011} cavities or low-noise shields can be manufactured.

(3) Film thickness can be as high as 100 μm and this has important consequences when high microwave power is required in a resonator.

(4) The films (at 50 μm) are always thicker than the penetration length, thus avoiding substrate dielectric loss effects.

2.6.2. Effect of microstructure on R_s. The surface resistance of YBCO thick films is strongly dependent on microstructure. Films sintered below the peritectic temperature are observed to have a surface resistance of 90 mΩ at 77 K and 18.5 GHz whereas films sintered by a melt-processing route above the peritectic temperature display R_s of 6 mΩ at 18.5 GHz and 77 K [5,6]. The microstructure of YBCO films prepared on zirconia substrates above and below the peritectic temperature has already been discussed. The effect of grain size and morphology on R_s is clear. In an earlier study on bulk materials Alford *et al* [62] demonstrated a relationship between grain size and R_s showing that larger grains resulted in lower R_s. Similarly it was shown that in thick films a grain size of a few microns gave R_s an order of magnitude higher than a grain size of the order of millimetres as seen in thick films displaying the growth of large spherulites [6].

2.6.3. Frequency dependence of the surface resistance. Conventional superconductors are well described by the two-fluid model [63]. This model assumes that a fraction x of the electrons in the film behave as electrons in the normal state while the remaining fraction act as superconducting electrons. The two-fluid model is expressed by

$$R_s = \tfrac{1}{2}\sigma_n\mu_0^2\omega^2\lambda^3 x \qquad (5)$$

where

$$\lambda = \lambda_0\left[1 - \left(\frac{T}{T_c}\right)^4\right]^{1/2} \qquad (6)$$

σ_n is the normal-state conductivity, μ_0 is the permeability of free space, $\omega = 2\pi f$, λ is the penetration depth and $x = (T/T_c)^4$.

The two-fluid model predicts that R_s can be given by equation (5) if the penetration depth is less than the normal skin depth, $\delta(= (\mu\omega\sigma/2)^{-1/2})$. Using equation (5) and substituting the values for R_s measured for thick-film YBCO [5,6,61] gives a 77 K value for the penetration length in YBCO with a T_c of 92 K and at a frequency of 18.5 GHz of approximately 3 μm. Calculations using a weakly coupled grain model or a resistively shunted junction model [64–66] give broadly similar results even although the applicability of the model of Remillard *et al* [64] does not include grain and shunt inductances and is limited to small-grained samples. In higher-quality samples which behave in a less granular manner these inductances must be included.

A value of 3 μm for the penetration depth is greater than that measured for thin films ($\lambda = 0.15$ μm) but less than the value calculated for large-grained bulk materials using data presented in [62] which is approximately 7 μm at 18.5 GHz and 77 K. Zhang *et al* [67] report a value of 50 μm in electrophoretically deposited YBCO films sintered below the peritectic temperature at 915 °C in O_2. The general trend appears to be a reduction in the calculated value for λ as the film quality improves. The argument here is that, for improved R_s, melt processing is required in order to improve film quality and that as film quality improves the penetration depth is reduced, approaching values measured for epitaxial thin films.

2.6.4. Microwave power effects. Non-linear response is manifested as an increase in R_s as microwave power is increased. The power may be represented in terms the response of Q (or R_s) to r.f. power or H_{rf}, the r.f. field [68]. Ghosh *et al* [68] and Cohen *et al* [69] also examined the influence of a background d.c. field on the r.f. power dependence finding that samples in which H_{rf} caused non-linearity at ~ 0.01 mT displayed non-linearity at ~ 0.1 T in d.c. fields, indicating that H_{rf} posed a far more serious problem than H_{dc}. It was also found that whereas intragranular pinning in thin films could be enhanced by Kr ion and α particle irradiation no change in the low H_{rf} dependence on the surface resistance was observed [69]. The work on thin films [70] shows that typically there is a gradual increase in R_s and λ as H_{rf} increases. This is a very common observation and has been interpreted in terms of a weakly coupled grain model already mentioned. One of the main problems with the stripline geometry when applied to thick films is the build-up of very high r.f. fields at the edges of the strip. The higher the Q of the structure, the larger the r.f. currents. Any attempt to manufacture high-Q structures using stripline techniques (e.g. [71]) suffers from the granularity of the film, the non-epitaxial growth, and the greatly reduced magnetic field resistance of thick films. In order to overcome these problems 3D resonators which by their geometry are very high-Q structures have been constructed. The results are surprisingly good as a result of three main factors. First the geometry of the structure is advantageous, second the film thickness (50 μm) is far thicker than that of a thin film by about a factor of 100 and third the processing techniques for the melt-processed films have advanced and continue to make considerable progress. The most important aspect by far is the modification of the processing so that the effect of granularity and weak links is considerably reduced. This is shown in figure 5 [72].

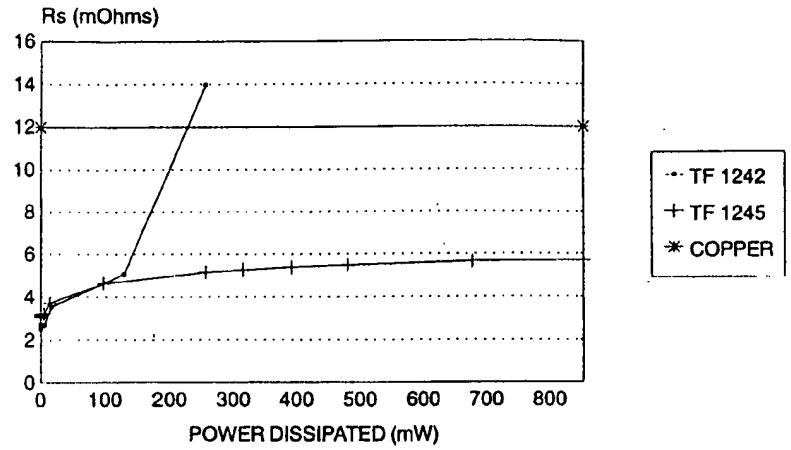

Figure 5. Effect of dissipated power on R_s of YBCO thick films. TF 1245 shows improved power performance as a consequence of modification in processing [72].

3. Applications of HTS thick films

3.1. HTS resonators

Current microwave communications base station filters are bulky and dissipate a considerable amount of power, and the filter response, in terms of rejection, is barely adequate. The rapid increase in the use of cellular communications and the projections for the next century indicate that present filters will not cope with the volume of calls. Novel filters are required which will cope with the increased volume. Thin-film circuits suffer from the problem of high current and field concentrations at the edge of patterned tracks. A manifestation of this problem is seen in the power handling of such films. Thick films can be used to coat TE_{011} cavities and, at 10, 7.5 and 5.6 GHz, unloaded Q values of 2×10^5, 5×10^5 and 7.6×10^5 respectively have been measured at 77 K. At 64 K the unloaded Q is 10^6 at 5.6 GHz. However, these cavities are far too large for practical applications; at 900 MHz such a cavity would require both diameter and length to be greater than 300 mm [72].

Cooling a series of such resonators is not practical and therefore smaller quasi-lumped element structures have been manufactured using YBCO thick films on polycrystalline zirconia substrates. Quasi-lumped element resonators allow structures to be made electrically small (width 90 mm, length 40 mm) and in HTS thick films Q values of over 100 000 at 77 K are recorded. Such Q values are sufficient for the construction of filters with low insertion loss and good rejection characteristics. A key performance requirement is the maintenance of Q as the microwave power is increased, as non-linearities in such devices are highly undesirable. The performance of these films is a significant improvement over earlier studies in which the samples were sintered below the peritectic temperature [62]. Below the peritectic temperature the surface resistance was found to be over an order of magnitude greater and the grain structure is quite different, i.e. smaller and poorly coupled grains. In comparison, films sintered above the peritectic exhibit far fewer grain boundaries per unit area and also possess a degree of preferred orientation. The study of high frequency losses [63–66] has suggested a weakly coupled grain model in which there is assumed to be Josephson coupling between the grains and in which the coupling is modelled using a resistively shunted junction. Given the differences in the grain microstructure of the films prepared below and above the peritectic temperature, the performance agrees qualitatively with the resistively shunted junction model for sintered materials where there is poor coupling between grains and where R_s is poor in comparison with melt-textured YBCO thick films [5]. In an early study of fine-grained sintered YBCO there was seen to be a well-defined power dependence in the material which, being fine grained, contained a large number of grain boundaries per unit volume [73]. It is now recognized that the coupling between the grains in such materials is poor. In melt-processed thick films, however, it is difficult to model the results in samples with similar microstructures (TF 1242 and TF 1245 in figure 5) but with very different power dependences. With reference to figure 5, TF 1242 shows an initial steep rise in R_s at low power, a region with lower slope and then a region where R_s rises rapidly as the power is increased. TF 1245, processed in a different manner but with a similar grain microstructure, shows an initial rise and then a flattening of the R_s versus power curve up to high power. It is difficult to explain this behaviour using such models. The results shown in figure 5 are for two samples with nominally identical grain structures but which have been subjected different processing conditions. It is suggested that the better power performance of sample TF 1245 is due to better coupling between the grains rather than simply a reduction in the grain boundary volume.

As well as the measurement of surface resistance, the measurement of the phase noise is of key importance. Preliminary measurements of phase noise have been carried out on a 7.5 GHz TE_{011} cavity in which both the barrel and endplates were coated with YBCO thick film [74]. The results are shown in table 3 [74]. It should be noted that the measured phase noise of the HTS cavity is now limited

Table 3. Phase noise for HTS thick-film oscillator [74].

Oscillator system	Measurement temperature (K)	Phase noise (dBc Hz^{-1}) 1 kHz offset	10 kHz offset
Cu cavity	300	−90	−120
Cu cavity	77	−95	−124
HTS cavity	77	−108	−135

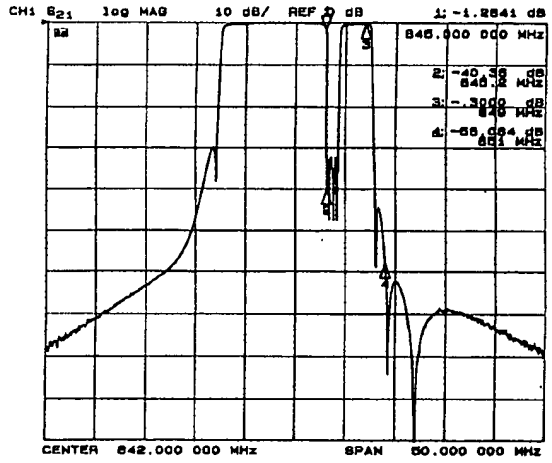

Figure 6. Performance of thick-film YBCO filters manufactured by Illinois Superconductor Corporation (ISC model Q45K-B3A, 10-pole elliptic bandpass with 6-pole quasi-elliptic notch; CDMA–TDMA–AMPS compatible). Insertion loss at markers 1 and 2 is −1.2 dB and −0.3 dB respectively and at markers 2 and 4 is −40.36 dB and −58.08 dB respectively demonstrating very low insertion loss and good rejection characteristics.

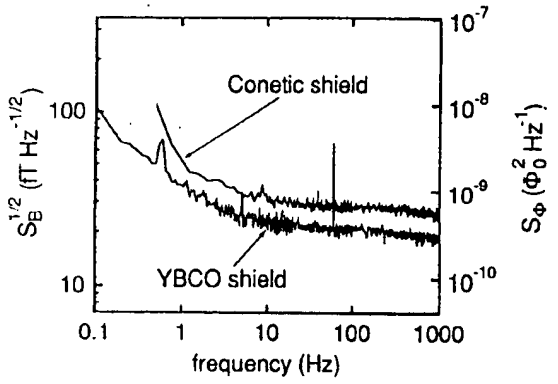

Figure 7. Noise characteristics of thin-film multiloop magnetometers enclosed within YBCO thick-film shields at 77 K [76].

by the noise floor of the measurement system. It is likely that the phase noise of HTS thick films is lower but more precise measurements involving an alternative experimental procedure will be required.

Recently the technology developed by Alford and Button [6] (now at South Bank and Birmingham Universities respectively) has been employed by Illinois Superconductor Corporation in high-performance filters for base station applications. The filter response using this technology is shown in figure 6 where it is seen that the filters possess very steep skirts and low insertion loss. The market demand for new products in this area is high with more than 20 million new cellular users in 1994. The huge increase in demand has caused increased call interference particularly in densely populated urban areas. Pre-selection filters, which minimize noise from adjacent bands, cause a loss of signal and increased insertion loss. By using HTS filters whose resonant elements have unloaded Q of 100 000, filters with exceptionally low insertion loss and high rejection have been manufactured. These are currently being tested at six test sites in the USA.

3.2. HTS shields

Shields can be made in HTS thick film on cylindrical zirconia substrates. For magnetoencephalography and magnetocardiography the three essential requirements of a shield are that it should be capable of excluding the earth's field (0.05 mT), the flux creep rate must be adequately low and the flux noise is low. The DC field rejection of a 40 mm thick film is approximately 0.5–1 mT at 77 K The creep rate of such films has been measured [75]. For a shielded area of 1 cm^2, a creep rate of 10^{-5} flux quanta s^{-1} can be shown to correspond to 2×10^{-20} V. At the lowest voltages, the measurements indicate that the flux creep is well below that required for shielding applications. This suggests the use of such shields in the provision of very low magnetic noise environments which are required for sensitive measurements using SQUIDs. The noise properties of YBCO–$SrTiO_3$–YBCO thin-film multiloop magnetometers enclosed within YBCO thick-film shields have been measured by Ludwig *et al* [76] and found to be very low at 37 fT $Hz^{-1/2}$ at 1 Hz and 18 fT $Hz^{-1/2}$ at 1 kHz. The results of this are shown in figure 7 [76]. In the experiment the devices were immersed in liquid nitrogen and a stable field was applied by winding a copper solenoid around the zirconia tube. The inside of the tube was coated with thick-film YBCO. The results of these series of experiments show that the critical properties (field exclusion, flux creep and magnetic noise) are all well within the measured performance of the YBCO thick films described here.

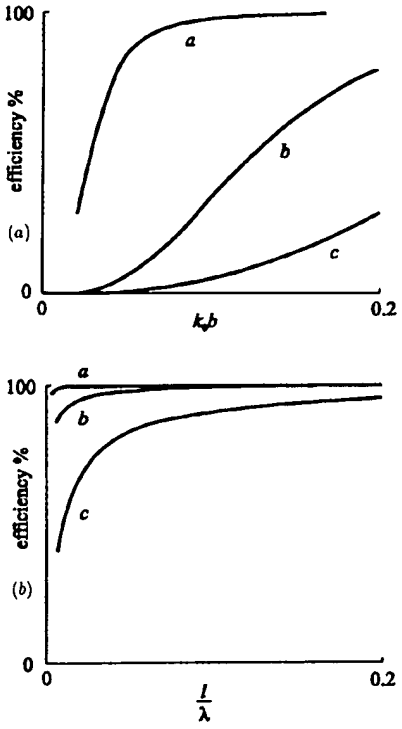

Figure 8. (*a*) Efficiency of a small loop antenna [81]. The superconductor is assumed to be a YBCO wire with a cross-over frequency (i.e. where R_s (copper)= R_s (YBCO)) of 10 GHz only. Curve *a*, HTS wire diameter 1 mm, 77 K; curve *b*, Cu diameter 1 mm 300 K; curve *c*, Cu diameter 0.1 mm, 300 K. $k_0 = 2\pi/\lambda$ and *b* is the loop radius. (*b*) Efficiency of a small dipole antenna with the same parameters as in (*a*) [81].

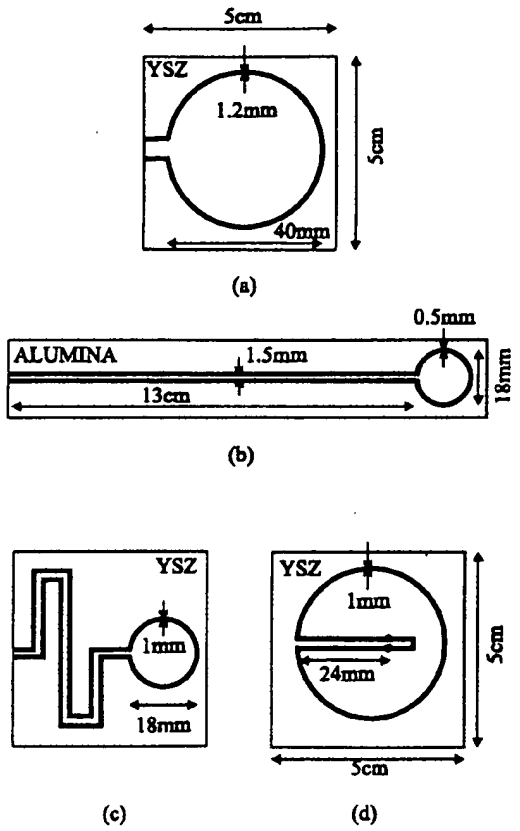

Figure 9. YBCO loop antennas and matching networks [79] with performance shown in table 4.

3.3. Antennas

The first demonstration of a HTS antenna was by Khamas *et al* [77] on an antenna made of bulk-extruded wire. Thick-film antennas have been extensively examined [78–83] and have been shown to offer certain advantages. The main advantage of a superconducting antenna is seen in figure 8 [81] where it can be seen that, for a given efficiency, the size of the antenna can be made very much smaller. It would be an advantage to print such antennas on a very low loss substrate such as alumina. Unfortunately, as discussed earlier, alumina reacts deleteriously with the superconductor, hence the reason for exploring novel substrate materials with lower dielectric loss which do not react adversely. The term electrically short is given to antennas with the radius of the smallest enclosing sphere being less than the radian length $\lambda_0/2\pi$. This means they are far smaller than the wavelength under consideration. In general very small electrically short antennas at microwave frequencies or higher are better constructed in thin films where very small antennas are an advantage [84]. However, for conformal antennas or helical antennas or for antennas where larger size or non-planar substrates are required then thick-film antennas can show an advantage.

Losses in small antennas occur at the feed and impedance-matching network and at the radiating element. For supercooled antennas the radiation resistance of the radiating element is often greater than the element loss resistance. In thick-film antennas, therefore, losses occur at the feeding–matching configuration, the finite surface resistance of the superconductor at a given frequency and the dissipation in the substrate. In addition performance can be degraded as a result of irregularities in the patterning, the connection to the main feed line and the use of lumped elements and baluns. However, given these constraints, the performance is remarkably good. In general both dipole antennas and loop antennas outperform their copper counterparts by approximately 6 dB at 77 K and at a frequency of about 100–500 MHz. The results of experiments by Ivrissimtzis *et al* [79] on a series of antennas as shown in figure 9 are summarized in table 4.

All the loop antennas with the exception of loop B have a higher than normal gain. Loop B is inferior as the substrate used was polycrystalline alumina which reacts adversely with the YBCO thick film at the sintering temperature used. Loops A, C and D use polycrystalline yttria-stabilized zirconia as the substrate which, despite a higher dielectric loss ($\tan\delta = 10^{-3}$–10^{-4}) produces a far better microstructure as mentioned above. Another advantage of the zirconia substrate is the dielectric constant which at 25 aids miniaturization in comparison with alumina whose dielectric constant is 10.

Table 4. Results for loop antennas [79].

Antenna type	Loop A	Loop B	Loop C	Loop D
Operating frequency (MHz)	259.2	428.3	412.4	139.6
Miniaturization factor	0.109	0.628	0.194	0.058
Relative bandwidth (%)	1.56	2.3	1.4	3.2
Q factor upper efficiency bound (%)	94.9	48.2	69.2	9.8
Supergain factor	6.2	0.4	2.3	1.2

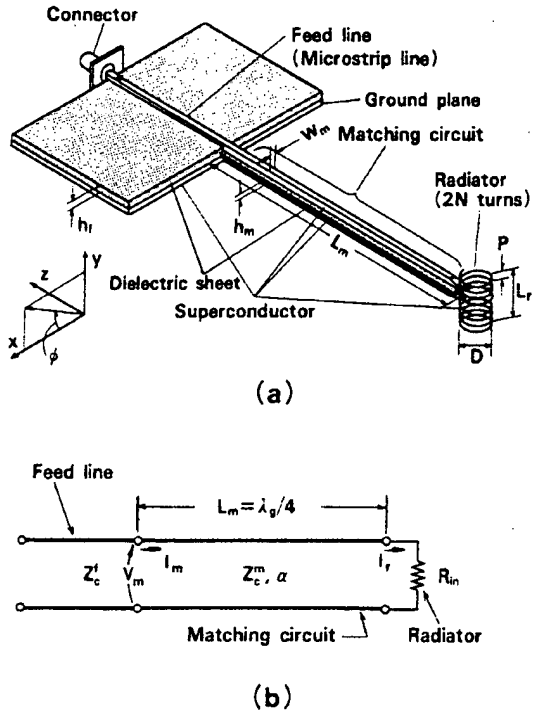

Figure 10. (*a*) Diagram of YBCO thick-film antenna with helical radiator and matching circuit [85]. (*b*) Equivalent circuit of antenna shown in (*a*).

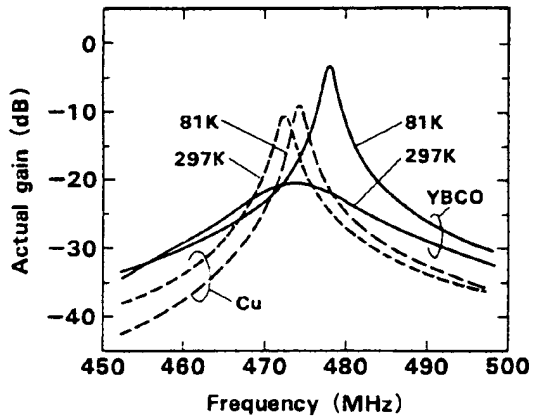

Figure 11. Performance of antenna shown in figure 10(*a*) [85].

Itoh *et al* [85] have examined a HTS electrically small ($\lambda/45$) helical antenna (manufactured by the authors NMcNA and TWB) as shown in figure 10(*a*). The helical radiator works as an electric dipole and is joined directly to a $\frac{1}{4}$ wave matching circuit. This is made from parallel transmission lines in a thick-film HTS. The design was intended to improve radiation efficiency and to increase the bandwidth. This was achieved as shown in figure 11 where it should be noted that the temperature of operation was 81 K, only 11 K below T_c.

3.4. Conductors using thick films

Dip-coated conductors using silver tapes on which the superconductor (BSCCO usually) is deposited have impressive properties. Tiefel and Jin [86], using $Bi_{1.6}Pb_{0.3}Sb_{0.1}Sr_2Ca_2Cu_3O_x$, show that transport J_c of 2.3×10^5 A cm^{-2} at 4.2 K and 8 T ($H_\perp a$–b) is achievable over a 2 cm length. Yang *et al* [87] show that in BSCCO 2212 electrophoretic deposition can be used to deposit material up to a few hundred microns although optimal results were seen at 100 μm. A J_c of 180 000 A cm^{-2} at 4.2 K in zero field was measured over 10 cm and this decreased to 120 000 A cm^{-2} in a 2 T field applied parallel to the face of the tape. Oxford Instruments (Cowey *et al* [88]) have evaluated the use of BSCCO thick films in dip-coated silver tape (DIP) and in dip-coated tape which is subsequently sheathed in silver (SSDIP). A 100 μm slurry is deposited onto a silver tape and wound and reacted. The sintered BSCCO thickness was around 30 μm. In the case of DIP tape the silver:superconductor ratio is 1:1 and in the case of SSDIP the ratio is 3:1. Short-sample (4 cm) results are shown in table 5.

Cowey *et al* [88] point out that there are severe problems in overcoming the length problem, i.e. the observed reduction in I_c and J_c as longer lengths of conductor are produced. Recent results from Oxford Instruments on dip-coated tapes indicate that $J_c = 4 \times 10^5$ A cm^{-2} are possible in lengths up to 20 cm and $J_c = 1 \times 10^5$ A cm^{-2} are achieved in lengths between 10 and 100 m.

Short samples of doctor-bladed BSCCO 2212 have been tested by Kase *et al* [89]. The BSCCO powder was mixed with an organic and a tape was placed onto a silver sheet. Various heating and cooling schedules were investigated but the composite heated to 890 °C and cooled to 870 °C at 5 °C h^{-1} and held for 1–24 h and then slowly cooled to room temperature displayed the best results. These were $J_c = 3.1 \times 10^5$ A cm^{-2} at 2 T and 4.2 K, 1.7×10^5 A cm^{-2}

Table 5. J_c and I_c of BSCCO tapes using thick films (SSDIP and DIP) [88].

		J_c (A cm^{-2} × 10^5) in ceramic core	J_c (A cm^{-2} × 10^3) full cross-section	I_c (A)
PIT	4.2 K, 0 T	2.0	67.0	101
PIT	4.2 K, 10 T	0.1	4.0	6.6
SSDIP	4.2 K, 0 T	9.1	5.4	328
SSDIP	4.2 K, 10 T	1.0	6.0	36
DIP	4.2 K, 0 T	2.2	90.0	439
DIP	4.2 K, 10 T	0.7	29.0	142

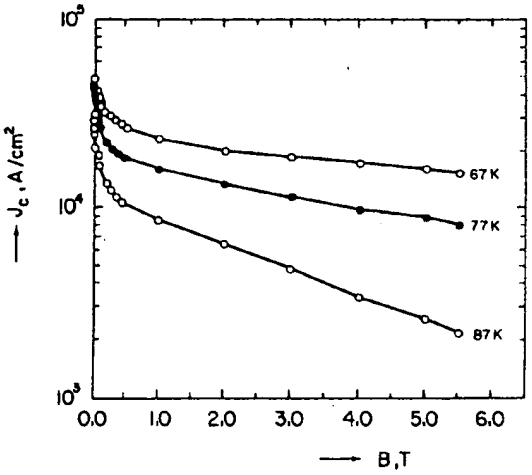

Figure 12. Transport J_c (T) of Tl-1223 deposited on a silver substrate by electrodeposition. $B_{\|}a$–b plane from reference [96]. See also reference [90].

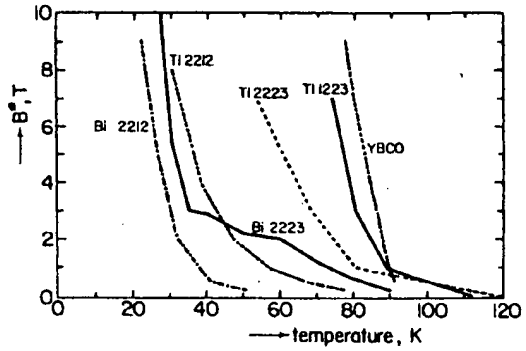

Figure 13. Irreversibility line for the three main HTS systems [90, 99].

10 T, 4.2 K and 1.4×10^5 A cm^{-2} at 4.2 K, 25 T. The field was applied perpendicularly to the current and parallel to the tape surface.

Thallium-based thick films have recently shown significant promise. For detailed information on such conductors the reader is referred to a comprehensive review by Jergel *et al* [90] in which methods such as electrodeposition, sol–gel, aerosol deposition and screen printing are described. Table 6 is adapted from Jergel *et al* [90] and shows Tl tapes in which thick films have been deposited by so-called 'open deposition' methods i.e. not PIT.

An example of the performance of tapes described in [96] is shown in figure 12. The results shown in figure 12 are for tapes which were prepared by electrodeposition [94]. The nitrate precursors without Tl were dissolved in dimethyl sulphoxide and deposited on 125 μm silver coil. A two-zone furnace was used with oxygen as a carrier gas for thallium oxide vapour. The zero-field value for J_c is 4.42×10^5 A cm^{-2} but high-field performance is impressive at $J_c = 8.2 \times 10^3$ A cm^{-2} at 5.5 T. The main reason for the interest in Tl materials is seen in figure 13 [90, 99]. The irreversibility line for the Tl 1223 and 2223 shows significant advantage over the BSCCO system.

3.5. Thin-film conductors using pulsed-laser deposition and ion-beam-assisted deposition

Although not strictly a thin film by the terms of the definitions set out at the beginning of the paper, YBCO 123 conductors prepared by pulsed-laser deposition and ion beam assisted deposition are certainly worthy of mention, first, because the irreversibility line for YBCO shows the greatest promise in comparison with BSCCO and TBCCO (figure 13) and, second, the properties over 40 mm tracks are excellent. Wu *et al* [1, 100], using thin nickel-based alloy substrates, have demonstrated biaxial texturing of YBCO using ion-beam-assisted deposition to deposit a textured CeO_2 buffer layer, a YSZ layer and pulsed-laser deposition to deposit the YBCO. The key to the achievement of high critical currents is the achievement of very low full width at half-maximum (FWHM) for the YBCO (103) peaks. At 75 K $J_c = 1 \times 10^6$ A cm^{-2} for a 1 μm thick film. The FWHM for this film is around 5°–6° and the properties are only a factor of 2–3 worse than those of a film of the same thickness deposited on CeO_2-buffered single-crystal YSZ. These remarkable properties allow 2 μm thick, 40 mm long, 10 mm wide conductors to be manufactured which show critical currents at 75 K of 120 A in zero field, and approximately 50 A in 1 T ($H_{\|}a$–b). The authors recognize that limitations of process speed and deposition area inhibit economic viability but the demonstration of feasibility is extremely encouraging and the properties measured are excellent.

Table 6. Results for thallium tapes prepared by open deposition methods (adapted from [90]).

Compound TBCCO	Method	Substrate	Film thickness (μm)	J_c transport (A cm^{-2} $\times$ 10^4), 77 K, 0 T	J_c transport in field (A cm^{-2} $\times$ 10^4), 77 K
1223 [91] T(B,S)CCO	Solution spray	YSZ	~ 3	2–11	0.7 (1 T)
1223 [92]	Solution spray	$SrTiO_3$/Ag	< 1	28	5 (1 T)
1223 [93]	Solution spray	YSZ	3	10	5 (0.1 T)
1223 [94] (T,P)(B,S)CCO	Solution spray	Ag tape	1	9	0.7 (1 T)
1223 [95]	Ink spray	$LaAlO_3$	5–20	2.9	> 1 (1 T)
2223 [14]	Electrodeposition	Ag	1.3	3.2	1 (1 T)
1223 [96]	Electrodeposition	Ag	1	4.42	0.82 (5.5 T)
1223 [97]	Electrodeposition	Ag	1	7	1 (5 T)
1223 [98]	Sol–gel	Ag	10–30	2.5	0.1 (1 T)

3.6. Magnetic resonance imaging receive coils

The first demonstration of the use of HTS receive coils was by Hall *et al* [101] using bulk materials. Thick-film coils are interesting as they have the potential for large area coverage, they can be 3D, their superconducting properties are better and they are far more robust. The use of thick YBCO films was first reported by Penn *et al* [102] where it was found that HTS thick-film coils showed improvements over a copper mimic at 77 K. However, the expected improvement, given an f^2 scaling in R_s and given that the frequency of operation was only a few MHz, was not realized. The reasons for this are believed to be a function of the geometry rather than any fundamental change in R_s at low frequency. The main objective is to increase the signal-to-noise ratio (SNR).

Traditionally [103], the SNR in an MRI system is given by

$$\psi \approx 8.4\nu^{7/4}/a$$

where ν is the frequency in megahertz and a is the radius of the coil in metres. This relation is for an optimized copper coil at room temperature where the body noise has been neglected. It is not valid for a superconducting coil as the frequency dependence of the resistance is different for copper ($R \propto \omega^{1/2}$) and a superconductor ($R \propto \omega^2$). In order to design an optimized HTS coil it is necessary to look at the factors affecting signal and noise more closely.

3.6.1. Signal. The amplitude of the free induction decay signal, the signal that is detected in MRI, is given by

$$\xi = \omega_0 \hat{B}_1 M_0 \Delta V \tag{7}$$

where ω_0 is the Larmor frequency and M_0 and ΔV are the magnetization and volume of the sample respectively. $\hat{B}_1$ is a coil geometry factor and is the field that would be produced by a unit current flowing in the coil. It is proportional to the number of turns in the coil n. The magnetization is proportional to the applied field (B_0) and thus to ω_0.

3.6.2. Noise. The Johnson noise places a lower limit on the size of a signal which may be detected in the presence of a resistance R. The root mean square of the random voltage is given by the Nyquist equation

$$N = (4kTR\,\Delta\nu)^{1/2} \tag{8}$$

where k is Boltzmann's constant, T is the temperature of the resistance and $\Delta\nu$ is the bandwidth of the measuring system. If the coil resistance (r_c) dominates R, then R increases linearly with n. Comparing equations (7) and (8) it would appear that one could increase the SNR by indefinitely increasing the number of turns in the coil as the signal is proportional to n and the noise is only proportional to $n^{1/2}$. However, other factors intervene to make it impossible to take this approach. A major factor is the speed of light. If the number of turns is too large, the length of the wire in the coil approaches the wavelength of the r.f. signal. This causes a phase shift in the signal as it moves round the coil which causes a decrease in signal. To avoid this it is generally accepted [104] that the length of the conductor should not exceed $\lambda/20$. This is a problem in high-field systems. For a low field at about 0.01 T or 420 kHz this length is about 35 m which for a coil of diameter around 100 mm gives a maximum of about 100 turns. This number of turns is currently above the practical limit in thick films owing to the high patterning definition required. This suggests that one way to improve the performance of low-field HTS coils is to increase the number of turns. A practical measure of the resistance of a coil is the quality factor Q. This is given by $Q = \omega L/r_c$.

3.6.3. Body noise. The coil resistance is not the only source of loss. The human body is a conductor, albeit a poor one, and thus is a source of resistance and loss. This loss shows up as reduction in the coil's Q which can be represented by an increase in the resistance r_m. r_m depends on the geometry of the coil and is proportional to ω^2 [103, 105] independent of geometry.

3.6.4. The frequency dependence of the SNR. From the above arguments it can be seen that the SNR ψ is given by

$$\psi \propto \frac{\omega_0^2 \hat{B}_1}{(r_c T_c + r_m T_m)^{1/2}} \tag{9}$$

since $r_m \propto \omega^2$ and, for a copper coil, $r_c \propto \omega^{1/2}$ at low frequencies r_c, i.e. the coil dominates the loss. It is in this region that the SNR can be improved by reducing the resistance of the coil, i.e. by using a superconductor. For a superconductor $r_c \propto \omega^2$, so whether the coil or body dominates the noise no longer depends on frequency. It is now dependent on the geometry and the resistance of the coil. The question now is, is the resistance of the superconductor so low that it is again the body noise that dominates and if so is there enough SNR for imaging?

To answer this question it is necessary to use some experimental data and then to extrapolate them to the proposed system. In order for the extrapolations to be valid the data must be from a system with a similar geometry. Bourne *et al* [106] give information on SNR and body noise for a 70 mm diameter HTS planar surface coil at 0.064 T (2.72 MHz). The body noise extrapolates to 1 mΩ at 0.01 T (426 kHz). At 77 K the coil had an r_c of 52 mΩ (which they admit is a long way from being optimized) and improved the SNR by a factor of 2.4 compared with the standard copper coil. For the purposes of this review, a coil designed and built by one of the authors (SJP) had $r_c = 40$ mΩ at 20 MHz which scales to 0.02 mΩ at 426 kHz (0.01 T). It is clear, therefore, that in this case the body noise will again dominate. This means that is possible to change the geometry of the coil in a way that would increase its resistance, i.e. more turns, narrower tracks, without adding to the noise. From equation (9) we can derive a figure of merit, Φ, which is proportional to ψ to compare the SNRs of different systems:

$$\Phi = \frac{\omega_0^2}{(r_c T_c + r_m T_m)^{1/2}}.$$

For the superconducting coil in reference [106], $\Phi = 6.7 \times 10^{13}$ which means that for the standard copper coil $\Phi = 2.8 \times 10^{13}$. From the figures for the HTS coil at 0.01 T we obtain $\Phi = 1.3 \times 10^{13}$ which is only a factor of 2 below a commercial coil currently in use. This value can be improved by improving the geometry of the coil, i.e. by increasing the number of turns, or by increasing the field a little since the proposed system is not constrained to exactly 0.01 T. If the field were 0.02 T then the SNR would match the copper value.

There are also more subtle considerations that help a low-field system. One is that SNR is not the best metric of image quality; it is the contrast-to-noise ratio (CNR) that makes an image useful. The CNR is basically the product of the SNR and the contrast which is dependent on the field. At low fields the contrast between different types of tissues is enhanced.

4. Conclusions

The materials, the processing and the devices have been discussed with reference to thick-film high-temperature superconductors. It was seen that there are three main material systems used to manufacture thick films: YBCO, BSCCO and TBCCO and their substitutional variants. The Hg system was also discussed. Each system is processed in a different manner. Melt-processed YBCO materials on partially stabilized zirconia substrates were seen to be most used as thick film for shields and r.f.–microwave applications owing to their low noise and R_s, and because of the potential for large area coverage on planar or 3D substrates. An interesting potential area is MRI receive coils which in principle show promise but which need to be demonstrated in a working system. It was seen that the key to improvement in these materials was the identification and use of new substrate materials. BSCCO was seen to be the material of preference at present for dip-coated thick-film wire or tape conductors where at 4.2 K it outperforms conventional superconductors at high magnetic fields. The thallium system is more problematic because of toxicity but thick films of TBCCO have displayed low R_s at low power. In addition, as a result of the encouraging performance in field of open tapes of TBCCO in comparison with BSCCO at 77 K there is interest in developing these materials as conductors. Finally, although not strictly a thick film given the definition at the outset of this work, it was seen that pulsed-laser deposition (of the YBCO) and ion-beam-assisted deposition (of the YSZ) thin-film processing was able to make YBCO films 1–2 μm in thickness capable of sustaining a J_c of 10^6 A cm^{-2} over a length of 40 mm.

References

[1] Wu X U, Foltyn S R, Arendt P, Townsend J, Adams C, Campbell I H, Tiwari P, Coulter Y and Peterson D 1994 *Appl. Phys. Lett.* **65** 1961–3

[2] Dou S X and Liu H K 1993 *Supercond. Sci. Technol.* **6** 297–314

[3] Sato K, Hikata T and Iwasa Y 190? *Appl. Phys. Lett.* **57** 1928

[4] Hikata T, Sato K and Hitotsuyanagi H 1989 *Japan. J. Appl. Phys.* **28** L82

[5] Alford N McN, Button T W, Adams M J, Hedges S, Nicholson B and Phillips W A 1991 *Nature* **349** 680–3

[6] Alford N McN and Button T W 1991 *Adv. Mater.* **30** 318–20

[7] Button T W, Alford N McN, Wellhofer F, Shields T C, Abell J S and Day M 1991 *IEEE Trans. Magn.* **27** 1434–7

[8] Wellhofer F, Day M J and Abell J S 1993 *Mater. Sci. Eng.* B **21** 19–25

[9] Bailey A, Alvarez G, Russell G J and Taylor K N R 1991 *Bull. Mater. Sci.* **14** 111–6

[10] Senda M and Ishii O 1991 *J. Appl. Phys.* **69** 6586–9

[11] He Q, Christen D K, Klabunde C E, Traczyk J E, Lay K W, Paranthaman M, Thompson J R, Goyal A, Padraza A J and Kroeger D M 1995 *Appl. Phys. Lett.* **67** 294–6

[12] Lay K W and Tkaczyk J E 1994 *Appl. Supercond.* **2** 677–84

[13] Su L Y, Grovenor C R M, Goringe M J, Dewhurst C D, Cardwell D A, Jenkins R and Jones H 1994 *Physica* C **229** 70–8

[14] Battacharya R N, Parilla P A and Blaugher R D 1993 *Physica* C **211** 475–85

[15] Remillard S K, Arendt P N and Elliott N E *Physica* C **177** 345–50

[16] Holesinger T G, Phillips D S, Coulter J Y, Willis J O and Peterson D E 1995 *Physica* C **243** 93–102

[17] Vandriessche I, Depla D, Denul J, Deroo N, Gryse R and Hoste S 1994 *Appl. Supercond.* **2** 391–400

[18] Hagberg J, Usimaki A and Leppavuori S 1993 *Appl. Supercond.* **1** 1091–8

[19] Dou S X, Liu H K, Bourdillon A J, Tan N X and Sorrell C C 1989 *Physica* C **158** 93–8
[20] May P, Jedamzik D, Boyle W and Miller P 1988 *Supercond. Sci. Technol.* **1** 1–4
[21] Koshy J, Kumar K S, Kurian J, Yadava Y P and Damodaran A D 1994 *Bull. Mater. Sci.* **17** 577–84
[22] Koshy J, Kurian J, Yadava Y P, Sajith P K, Damodaran A D, Rai S P, Dhananjayakumar, Pinto R and Vijayaraghavan R 1994 *Physica* C **225** 101–4
[23] Koshy J, Thomas J K, Kurian J, Yadava Y P and Damodaran A D 1993 *Physica* C **215** 209–12
[24] Kurian J, Koshy J K, Wariar P R S, Yadava Y P and Damodaran A D 1995 *J. Solid. State Chem.* **116** 193–8
[25] Koshy J, Thomas J K, Kurian J, Yadava Y P and Damodaran A D 1993 *Mater. Lett.* **15** 298–301
[26] Koshy J, Kumar K S, Kurian J, Yadava Y P and Damodaran A D 1994 *Appl. Phys. Lett.* **65** 2857–9
[27] Thomas J K, Koshy J, Kurian J and Damodaran A D 1995 *Supercond. Sci. Technol.* **8** 525–8
[28] Paulose K V, Koshy J and Damodaran A D 1992 *Physica* C **193** 273–6
[29] Zhang J L and Evetts J E 1994 *J. Mater. Sci.* **29** 778–85
[30] Koshy K S, Kumar J, Kurian J, Yadava Y P and Damodaran A D 1994 *Physica* C **234** 211–8
[31] Bhattacharya D, Roy S N, Basu R N, Dassharma A and Maiti H S 1993 *Mater. Lett.* **16** 337–41
[32] Masuda Y, Matsubara K, Ogawa R and Kawate Y 1992 *Japan. J. Appl. Phys.* Part 1 **31** 2709–15
[33] Ezura E *et al* 1993 *Japan. J. Appl. Phys.* Part 1 **32** 3435–41
[34] Schulz D L, Parilla P A, Gopalswamy H, Swartzlande A, Duda A, Blaugher R D and Ginley D S 1995 *Mater. Res. Bull.* **30** 689–97
[35] Vanolo M Pavese F, Giraudi D and Bianco M 1994 *Nuovo Cimento Soc. Ital. Fis.* D **16** 2119–26
[36] Os'kina T E, Kazin P E and Tretyakov Yu D 1991 *Supercond. Sci. Technol.* **4** 301–5
[37] Kuczynski G C 1949 *J. Met.* **1** 169
[38] Frenkel J 1945 *J. Phys.* (USSR) **9** 385–91
[39] Exner H E and Petzow G 1973 *Sintering and Catalysis* ed G C Kuczynski (New York: Plenum) pp 279–93
[40] Shin M W, Hare T M, Kingon A I and Koch C C 1991 *J. Mater. Res.* **6** 2026
[41] Oka K, Nakane K, Ito M, Saito M and Unoki H 1988 *Japan. J. Appl. Phys.* **27** L1065–7
[42] Maeda M, Kadoi M and Ikeda T 1989 *Japan. J. Appl. Phys.* **28** 1417–20
[43] Bourdillon A and Tan Bourdillon N X 1994 *High Temperature Superconductors: Processing and Science* (New York: Harcourt Brace Jovanovich)
[44] Shi D, Chen J G, Xu M, Kourous H E, Fang Y, Li Y H and Boley M S 1990 *Supercond. Sci. Technol.* **3** 457–63
[45] Jones A R, Cardwell D A, Ingle N J C, Ashworth S P, Campbell A M, Alford N McN, Button T W, Wellhofer F and Abell J S 1994 *J. Appl. Phys.* **76** 1720–5
[46] Cardwell D A, Jones A R, Ingle N J C, Campbell A M, Button T W, Alford N McN, Wellhofer F and Abell J S 1994 *Cryogenics* **34** 671–7
[47] Ingle N J C, Cardwell D A, Jones A R, Wellhofer F and Button T W 1995 *Supercond. Sci. Technol.* **8** 282–90
Dewhurst C D, Cardwell D A and Alford N McN 1995 *Appl. Phys Lett* **77** 2067
[48] Langhorn J, Bi Y J and Abell J S 1996 *Physica* C **271** 164–170
Langhorn J B 1996 *Platinum Met. Rev.* **40** 64–9
[49] Jones A R, Baker A P, Dewhurst C D, Ashworth S P, Cardwell D A and Campbell A M 1995 *Appl. Supercond.* **3** 47–53
[50] Yang M, Goringe M J, Grovenor C R M, Jenkins R and Jones H 1994 *Supercond. Sci. Technol.* **7** 378–88
[51] Holesinger T G, Phillips D S, Coulter J Y, Willis J O and Peterson D E 1995 *Physica* C **243** 93–102
[52] Dimesso L, Masini R, Cavinato M L, Fiorani D, Testa A M, and Aurisicchio C 1992 *Physica* C **203** 403–10
[53] Suyiama A, Yoshimoti T, Endo H, Tsuchiya J, Kijima N, Mizuno M and Oguri Y 1988 *Japan. J. Appl. Phys.* **27** L542
[54] Takano M, Takada J, Oda K, Kitaguchi H, Miura Y, Ikeda Y, Tomii, Y and Mazaki H 1988 *Japan. J. Appl. Phys.* **27** L1041
[55] Gao W, Li S C, Rudman D A and Vandersande J B 1990 *Physica* C **167** 395
[56] Gao W, Li S C, Parrella R, Rudman D A and Vandersande J B 1990 *J. Mater. Res.* **5** 2633
[57] Chaudhry S, Khare N and Gupta A K 1992 *J. Mater. Res.* **7** 2027
[58] Schultz D L, Parilla P A, Ginley D S , Voight J A, Roth E P and Venturini E L 1995 *IEEE Trans. Appl. Supercond.* **5** (part 2) 1962–5
[59] Goyal A, Specht E D, Wang Z L, Kroeger D M, Sutcliff J A, Tkaczyk J E, Deluca J A, Masur L and Riley G N 1994 *J. Electron. Mater.* **23** 1191–7
[60] Tsabba Y and Reich S 1995 *Physica* C **254** 21–5
[61] Button T W and Alford N McN 1992 *Appl. Phys. Lett.* **60** 1378–80
[62] Alford N McN, Button T W, Peterson G E, Smith P A, Davis L E, Penn S J, Lancaster M J, Wu Z and Gallop J C 1991 *IEEE Trans. Magn.* **27** 1510–8
[63] Gorter C J and Casimir H B G 1934 *Physica* **1** 306
[64] Remillard S K, Reeves M E, Rachford F J and Wolf S A 1994 *J. Appl. Phys.* **75** 4103–8
[65] Hylton T L, Kapitulnik A, Beasley M R, Carini J P, Drabeck L and Gruner G 1988 *Appl. Phys. Lett.* **53** 1343–5
[66] Portis A M 1992 *J. Supercond.* **5** 319–30
Portis A M and Cooke D W 1993 *Mater. Sci. Forum* **130–2** 315–48
[67] Zhang B, Fabbricatore O, Gemme G, Musenich R, Parodi R and Capobianco P 1992 *Physica* C **203** 51–8
[68] Gosh I S, Cohen L F, Thomas J V, MacManus-Driscoll J L, Somekh R, Lenkens M, Hensen S, Muller G, Jedamzik D, Ren Z F, Wang C A, Wang J H, Gallop J C and Caplin A D 1995 *Applied Superconductivity 1995 (Inst. Phys. Conf. Ser. 148)* part 2, ed D Dew-Hughes (Bristol: Institute of Physics Publishing) pp 1083–6
[69] Cohen L F, Cowie A, Gallop J C, Ghosh I S, Chrosch J and Goncharov I N 1996 *Applied Superconductivity Conf. (Pittsburgh, 1996)* at press
[70] Oates D E, Nguyen P P, Dresselhaus G, Dresselhaus M S and Chin C C 1993 *IEEE Trans. Appl. Supercond.* **3** 1114–8
[71] Mossavati R, Gallop J C, Radcliffe W J, Button T and Alford N McN 1991 *IEEE Trans. Magn.* **27** 2952–4
[72] Penn S J, Button T W, Smith P A and Alford N McN 1995 *Applied Superconductivity 1995 (Inst. Phys. Conf. Ser. 148)* part 2, ed D Dew-Hughes (Bristol: Institute of Physics Publishing) pp 1051–4
[73] Peterson G E, Stawicki R P and Alford N McN 1989 *Appl. Phys. Lett.* **55** 1798–800
[74] Button T W, Smith P A, Alford N McN, Greed R B, Adams M J and Nicholson B F 1997 *IEEE Trans. Supercond.* at press
[75] Muirhead C M, Wellhofer F, Button T W and Alford N McN 1993 *IEEE Trans. Appl. Supercond.* **3** 1695–7
[76] Ludwig F, Dantsker E, Kleiner R, Koelle D, Clarke J, Knappe S, Drung D, Koch H, Alford N McN and Button T W 1995 *Appl. Phys. Lett.* **66** 1418–20
[77] Khamas S K, Mehler M, Maclean T S M, Gough C, Alford N McN, and Harmer M 1988 *Electron Lett.* **24** 460–1
[78] Wu Z, Mehler M J, Maclean T S M, Lancaster M J and Gough C E 1989 *Physica* C **162–4** 385–6
[79] Ivrissimtzis L, Lancaster M J, Maclean T S M and Alford N McN 1994 *IEEE Trans. Appl. Supercond.* **4** 33–40

[80] Ivrissimtzis, L, Lancaster M J, Maclean T S M and Alford N McN 1994 *IEEE Trans. Antennas Propag.* **42** 1–11
[81] Lancaster M J 1997 *Passive Microwave Device Applications of High Temperature Superconductors* (Cambridge: Cambridge University Press)
[82] Lancaster M J, Wu Z, Maclean T S M and Huang Y 1992 *IEE Proc.* H **139** 624
[83] Huang Y, Lancaster M J, Wu Z and Alford N McN 1991 *Physica* C **180** 267–71
[84] Chaloupka H, Klein N, Peiniger M, Piel H, Pischke A and Splitt G 1991 *IEEE Trans. Microwave Theory Tech.* **39** 1513–21
[85] Itoh K, Ishii O, Koshimoto Y and Cho K 1992 *IEICE Trans. Electron.* E **75C** 246–50
[86] Tiefel T H and Jin S 1991 *J. Appl. Phys.* **70** 6510–2
[87] Yang M, Goringe M J, Grovenor C R M, Jenkins R and Jones H 1994 *Supercond. Sci. Technol.* **7** 378–88
[88] Cowey L, Timms K, McDougall I, Marken K, Dai W and Hong S 1994 *Cryogenics* **34** 813–6
[89] Kase J L, Togano K, Kumakura H, Dietderich D R, Irisawa N, Morimito T and Maeda H 1990 *Japan. J. Appl. Phys.* **29** L1096–9
[90] Jergel M, Conde Gallardo C, Falcony Guajardo C and Strbik V 1996 *Supercond. Sci. Technol.* **9** 427–46
[91] DeLuca J A, Karas P L, Tkaczyk J E, Bednarczyk P J, Garbuskas M F, Briant C L and Sorensen D B 1993 *Physica* C **205** 21
[92] Doi T J, Yuasa T, Ozawa T and Higashiyama K 1994 *Japan. J. Appl. Phys.* **33** 5692–6
[93] Tkaczyk J E, Sutcliff J A, DeLuca J A, Bednarczyk P J, Briant C L, Wang Z L, Goyal A, Kroeger D M, Lowndes D H and Specht E D 1995 *J. Mater. Res.* **10** 2203
[94] 1995 Hitachi reports 1-meter Tl-2223 tape made by spray pyrolysis *Supercond. Week* **9** 1–2
[95] Schulz D L, Parilla P A, Ginley D S, Voigt J A and Roth E P 1994 *Appl. Phys. Lett.* **65** 2472
[96] Bhattacharya R H, Duda A, Ginlet, D S, DeLuca J A, Ren, Z F, Wang C A and Wang J H 1994 *Physica* C **229** 145
[97] Parilla P A, Schulz D L, Bhattacharya L, Blaugher R D, Ginley D S, Voigt J A, Roth E P and Venturini E L 1995 *IEEE Trans. Appl. Supercond.* **5** 1958
[98] He Q, Christen D A, Klabunde C S, Tkaczyk J E, Lay K W, Paranthaman M, Thompson J R, Goyal A, Pedraza A J and Kroeger D M 1995 *Appl. Phys. Lett.* **67** 294
[99] Blaugher R D 1993 *Processing and Properties of High Tc Superconductors I* (Singapore: World Scientific) p 271
[100] Wu X D *et al* 1995 *Appl. Phys. Lett.* **67** 2397–9
[101] Hall A S, Alford N McN, Button T W, Gilderdale D J, Gehring K A and Young I R 1991 *Magn. Reson. Med.* **20** 340–3
[102] Penn S J, Alford N McN, Hall A S, Button T W, Johnstone R, Zammattio S J and Young I R 1995 *Appl. Supercond.* **1** 1855–61
[103] Hoult D I and Lauterbur P C 1979 *J. Magn. Reson.* **34** 425–33
[104] Chen C-N and Hoult D I 1989 *Biomedical Magnetic Resonance Technology, (Medical Science Series)* (Bristol: Hilger) p 124
[105] Chen C-N and Hoult D I 1989 *Biomedical Magnetic Resonance Technology, (Medical Science Series)* (Bristol: Adam Hilger) pp 128, 160
[106] Bourne L C, van Heteren J G, Aidnik N O, Fenzi N O and James T W 1994 *Proc. Society of Magnetic Resonance (San Francisco, CA, 6–12 August 1994)*